To appear in *Liquid Crystals*
Vol. 00, No. 00, Month 20XX, 1–10

GUIDE

Microscopic characterization of self-assembled colloidal particles in electrohydrodynamic convection of a low-birefringence nematic liquid crystal

Yoriaki Nishioka[a], Fumiaki Kobayashi[a], Nobutaka Sakurai[a], Yuji Sasaki[a]*, and Hiroshi Orihara[a]

[a] *Division of Applied Physics, Faculty of Engineering, Hokkaido University North 13 West 8, Kita-ku, Sapporo, Hokkaido 060-8628 (Japan)* ;

(*v2.1 released January 2014*)

Electrokinetics of small particles immersed in anisotropic fluids is attracting attention in recent years. Here we focus on microscopic appearance of single as well as self-assembled particles moving in the electrohydrodynamic convection (EHC) of a nematic liquid crystal with low-birefringence. Characterization of the birefringent properties is made by polarized light microscopy under different illumination conditions. Because of the small optical anisotropy, the director distortion around the particles clearly exhibits distinctive colors on both sides depending on the height in the cell. The observation can be explained as the change in the net phase retardation of the light. It is also found that a caterpillar-like motion is possible by tuning temperature, although the horizontal size of the EHC rolls is relatively narrow.

Keywords: nematic liquid crystals; electrohydrodyanamic convection; liquid crystal colloids; electrokinetics

1. Introduction

Nematic liquid crystals (NLCs) formed by rodlike molecules are an anisotropic fluid with a long range orientational order of the long molecular axis. [1] The average orientation, called the director, can be controlled by the external electric or magnetic field and the surface anchoring. The anchoring effect appears not only at the substrates confining the sample but also around tiny inclusions immersed in NLCs. The dispersion of microparticles in NLCs has been an interesting colloidal system for the past two decades. [2–4] As is well known, when the NLC molecules align perpendicular to the surface of spherical particles, the asymmetric director distortion forms an elastic dipole due to the appearance of the topological point defect. Because of the elastic interactions generated between particles, self-assembled colloidal structures are possible from one to three dimensions. [5–7] Moreover, the symmetry breaking of the director field by the elastic dipole plays an important role for the dynamic behavior under electric fields. Recently an interesting electrophoretic motion, referred to as "liquid crystal enabled electrophoresis" (LCEEP) [8–10] is found for the dipolar colloids, which is due to the asymmetric "induced charge osmotic flow" (ICEO) around the particles. [11–13] Electrokinetic motion of particles is attracting attention from liquid crystal research [14–17] and is closely related to the liquid crystal microfluidics. [18, 19]

Particularly, for the NLCs with negative dielectric anisotropy, it is also possible to induce an electrohydrodynamic convection (EHC) by applying the electric fields above the threshold. [20, 21] Thus, the motion of particle is driven by both the LCEEP and the hydrodynamic flow of EHC. Recently it is found that the chain of elastic dipoles shows a directed caterpillar-like motion in EHC. [22, 23] This system provides a unique nature that enables a motion of self-assembled particles

*Corresponding author. Email: yuji.sasaki@eng.hokudai.ac.jp

whose deformation occurs out of the focal plane of the microscope. Such collective dynamics is a topic of general interest from experimental and theoretical perspectives. [24, 25] On the other hand, the NLC material used in earlier reports [22, 23] is limited to MBBA ((4-methoxybenzylidene)-4-butylaniline). It is interesting to explore other systems to obtain further information. In this work we report results on the colloidal dynamics in the EHC of a low-birefringence NLC material. The effect of the optical anisotropy of NLC for the microscopic appearance is studied. It is found that the use of λ-plate leads to characteristic colors around the particles, which reflects the height of particles, i.e., the change in the net retardation in the direction of sample thickness.

2. Experiment

We use trans, trans-4, 4′-dialkyl-(1α, 1′α-bicyclohexyl-4β-carbonitriles (CCNs, Nematel). [26] A series of homologue compounds possess negative dielectric anisotropy $\Delta\epsilon = \epsilon_{\|} - \epsilon_{\perp} \sim -5$.[27] The symbols $\|, \perp$ denote parallel and perpendicular components to the director. It is also known that the optical anisotropy is relatively low $\Delta n = n_{\|} - n_{\perp} \sim 0.03$. [27] We prepare a 50:50 mixture of CCN-47 and CCN-55 which shows nematic phase at room temperature. [28] A small amount of the ionic compound (tetrabutyl anmonium benzoate, Aldrich) is doped into the LC mixtures to induce electrohydrodynamic effects. Silica micro spheres ($2R = 2.47\mu$m, Bangs laboratories) are used as colloidal inclusions. Surface-modification is made using a silane-coupling agent, DMOAP (N,N-Dimethyl-N-octadecyl-3-aminopropyltrimethoxysilyl chloride) for homeotropic anchoring of NLC molecules around the particles. Commercial glass sandwich cells (EHC Co.) are used for experiments. The surface of indium tin oxide (ITO) coated glass substrates has a unidirectionally rubbed polyimide layer to induce the uniform planar anchoring. The cell gap, d is around 28 μm, determined by standard interference technique. AC voltage, $V = V_0 \cos(2\pi f t)$ generated from a function generator is amplified and is applied normal to the substrates (i.e. z-direction). The maximum value of the applied voltage is V_0=40 V. The observation is made using a polarizing microscope (Olympus BX 51) with illumination from a halogen bulb. The cell is set under the polarizing microscope, also equipped with a temperature controller. The experiments are done under different illumination conditions and the behavior is recorded using a DSLR camera (Sony ILCE-7R).

3. Results

We study the state diagram of samples for different ionic concentrations as a function of applied frequency f and voltage V_0. The emergence of convective flow by a moderate field, accompanies a spatial deformation of the director field inside the roll. [1, 21] This leads to the stripe pattern perpendicular to the rubbing direction under polarizing microscope, often referred to as Williams domains. [1, 20] The data in Figure 1(A) and (B) show the threshold voltage V_0^{th} for the Williams domains whose typical micrograph is shown as Figure 1(C). The letter P denotes the polarizer which is set to be parallel to the rubbing direction. It is seen that the curves for V_0 shift to high-frequency region by increasing the ionic concentration and temperature. As the frequency increases, the required threshold tends to be high as a whole. The behavior is quite analogue to that of well-studied compounds such as MBBA. [1, 21] At lower frequencies $\sim$ 20 Hz or below, V_0^{th} becomes slightly high, which is probably due to the electrostatic shielding by ions. The horizontal width of the single roll, which corresponds to the half wavelength of the director modulation, is typically 9 μm in the low frequency range. The contrast of the stripe pattern is weak because of the small Δn. The value is smaller than that of MBBA $\sim$ 15 μm in the earlier report [22] where the same commercial cells are used. It is also found that the temperature does not change the width so much. Thus, the cross section of the EHC roll is 9 μm wide and 28 μm high, i.e, the shape is quite elongated to z-direction. In addition, the roll width becomes shorter with the increase of V_0.

Here it must be mentioned that the threshold at high frequencies considerably changes over time possibly due to degradation of sample or ionic impurities from the alignment layer or electrodes, while little temporal and noticeable effects are found at low frequencies. Thus, our experiments are mainly carried out at 20 Hz to make sure of a relatively stable threshold and wider rolls. We tried to expand the width of EHC rolls by mixing other liquid crystals, keeping low birefringent property. However, since it was not so successful, we decided to use the present system.

The motion of single particles is checked by varying the strength of the electric fields $E_0 = V_0/d$. The following results displayed are obtained for the sample containing 1 wt% ions. Since the behavior in actual experiments is location-dependent, it is preferable to observe the same viewing area of the cell to obtain a consistent result. On the other hand, during observation, single particles self-assemble over time into a chain structure and eventually cannot be found efficiently in the cell. To repeat measurements, higher electric fields are occasionally applied in order to disassemble particles by inducing the turbulent flow. The hydrodynamic flow is strong enough to separate the connected particles in this system. Figure 2(A) shows micrographs without an electric field under different illumination conditions (A; analyzer, λ; λ-plate). Because of the low birefringence, it is difficult to discern the point defect around the particle under plane polarized light. The position can be judged under cross-polarized condition through the asymmetric director distortion as shown in the schematic illustration. The gray color seen around the particle indicates the low birefringence of the NLC. The distortion turns different colors on both sides of the particle with respect to the axis of symmetry by the insertion of λ-plate. Here, it should be noted that the observed colors are quite sensitive to particles' height. Thus, they only show the same appearance when the particles are at the equilibrium height balanced by the gravitational, buoyant, elastic repulsive forces. [29] A typical behavior of the x-directional velocity, v is shown in Figure 2(B) for two different temperatures. It is seen that the speed increases at high temperatures in the whole frequency range. When the electric field below V_0^{th}/d is applied, the particles exhibit ac electrophoresis motion, namely, LCEEP. They move in the opposite direction to the point defects, i.e, in the positive x-direction in coordinates of Figure 2(A). The velocity v increases nonlinearly $v \propto E_0^2$ due to the property of the LCEEP. [30] As the field strength increases, the color around the particle with λ-plate in place changes (Figure 2(C)), while the change of the focus of the particle image itself cannot be noticed clearly with our eyes. The color of the distorted area returns very slowly the original one of $E_0 = 0$ after the field is switched off. Thus, the possibility of the direct influence of electric fields on the nematic director distortion is ruled out, i.e., the height of particle is slightly different. This can be clearly confirmed with an onset of EHC where x-directional speed significantly increases with the regular undulation. Snapshots of a particle moving to the neighboring roll are shown in Figure 2(D) (see also supplementary Movie 1). The focus of the microscope is adjusted to the top side of the cell. The images for $t = 0$ s and $t = 38/60$ s correspond to the situation where the particle is at the bottom and top sides in the cell. Various changes in color are seen on both side of the particle. By comparison, it is seen that the appearance of the levitating colloid without an electric field (Figure 2(A)) corresponds to $t =\sim 12/60$ s. To obtain the qualitative data, confocal microscopic measurements would play a complementary role.

Since the observation of single particles with the use of λ-plate leads to marked behavior due to the regular undulating motion in z-direction, we further study the dynamics of colloidal chains of our most interest. In this system, we prepare the colloidal chains utilizing their self-assembling properties without a laser tweezers technique. The schematic illustration of our procedure is given in Figure 3(A). First a sample without colloids is introduced into the cell by capillary action in order to fill more than half area. Then another one containing relatively dense particles is subsequently added. If the electric field high enough above the threshold value is applied, because of the turbulent EHC flow, the particles can be disassembled and move in the opposite direction from the center of the particle to the point defect. Finally it is possible to separate particles depending on the direction of the point defects. Once the external field is switched off, the particles start to assemble again and form the chain structure (see also the image of Figure 3(A)). In contrast to the present system, the way described here is not so efficient for MBBA. The flow speed of EHC, the size

of the roll, and the elasticity probably make some difference. As an example, images for a chain consisting of $\sim$ 70 elastic dipoles are shown in Figure 3(B). The length is 193 μm. Likewise, the low birefringent property of the NLC makes it difficult to find the direction of the point defects around particles when only the polarizer is used. Cross-polarized illumination helps distinguish the direction by comparing two ends.

In the experiments, the electric field is gradually increased from small V_0 value. A noticeable finding of this system is that the undulation of the colloidal chain is seen even in the voltage lower than V_0^{th} of the state diagram. The onset voltage for the deformation depends on the length of the chain. The longer colloidal chain tends to undulate with a small voltage. For example, in an experiment at the room temperature, the chain in Figure 3(B) exhibits an undulating structure accompanying the caterpillar motion from $V_0 \sim 9$ V $\ll V_0^{th} \sim 22$ V (see Figure 1(B)). Figure 3(C) is taken with $V_0 \sim 11$ V. The x-directional speed is comparable to the electrophoretic one of single particles. Under the same condition, single particles and shorter chains (typically consisting of fewer than 10 particles) only show the electrophoretic motion. Although the reason for the instability appearing for longer chains is not clear, it might be an independent of liquid crystal properties. The addition of λ-plate leads to an interesting appearance in comparison to that without undulation. The four colored regions around the chain are understood by combining the orientation of the director and the height of particles. Crudely we estimate the amplitude of the undulation. In the figure, the apparent length in x-direction amounts 136 μm, i.e., the observable length amounts to 70 % of the original one. By assuming the colloidal chain as a shape of sine curve, the amplitude of the undulation is around 7 μm. Further increase of V_0, however, cannot lead to the further undulation. It is difficult especially for longer chains to realize the caterpillar motion in visible Williams domains. They are trapped in the EHC rolls. This is, as displayed in Figure 1(C), because the roll width ~ 9 μm is short compared to the cell gap 28 μm. It can be expected that that the narrow x-directional spacing restricts the movable region for particles. Forming the caterpillar structure requires sharp deformation of connecting particles, which is irrespective of the diameter. The elastic attractive interaction decreases as the orientation of the chain to the director fields (i.e., x-axis) increases.

Moreover, we study the motion of chains at a higher temperature of 39.5°C. As shown in Figure 2(B), the faster transportation is possible for single particles in the EHC. This make us expect more efficient motion even for chains and indeed some improvements are found. For the very long chain such as shown in Figure 3(B), a faster motion than that in the room temperature is obtained (Figure 4(A) and (B)) and the apparent length can be shorter than that of 25.5 °C ($\sim$ 60 % of the original chain). Below the undulation, the speed is very slow, while it increases suddenly with the onset of the EHC flow around it. The similar nature is observed for MBBA. [22] However the structure still cannot be maintained in Williams domains. On the other hand, we found that chains with moderate length consisting of $\sim$ 30 particles or fewer can exhibit a caterpillar-like motion in Williams domains. The snapshots are shown in Figure 5. The apparent length observable from microscopy reduces to be $\sim 1/3$ of the original length, i.e., the deformation is quite large in z-direction. Because of this large undulation, the image is not so clear under cross-polarized condition. Contrary to the long chain with smaller undulation, vivid color change is not seen. The particles move quite smoothly and fast (see supplementary Movie 2). From the figure, it is seen that one cycle takes shorter than 2 seconds. However, the EHC rolls around the chain tend to move to the opposite direction of the moving direction, while the other area exhibits more stationary domains. Thus, the speed of the transportation is not so fast, which is also seen from the figure. The observation implies that adjusting detail experimental condition is crucial for the mobility and shows the possibility for persistent transport of long chains in observable EHC regions.

4. Discussion

Generally, the typical EHC mechanism is considered for samples with negative dielectric, $\Delta\epsilon < 0$ and positive conductive, $\Delta\sigma > 0$ anisotropies. In the following, we use a notation $(\Delta\epsilon, \Delta\sigma) = (\pm, \pm)$ to denote material properties. For cells with the planar alignment, the combination of $(-, +)$ can cause an instability playing the central role for EHC. On the other hand, it is reported that CCN-47 compound has a negative conductivity anisotropy, i.e. $(-, -)$. [31] Indeed, we do not observe the EHC rolls when the NLC mixture is used as it is without mixing ions. According to the conventional understanding, such compounds cannot exhibit the instability. Recent studies of electrical instability on the $(-, -)$ compounds suggest that the flexoelectric effect causes the non-standard electrohydrodynamic convection whose roll is parallel to the rubbing direction. [32–34] Considering the above, one possible reason for the emergence of the standard EHC roll could be the effect of the doped ions. It is known that the electrical conductivity is quite sensitive to the type of mixed ions. Impurity flips the sign of the anisotropy $\Delta\sigma$. [35] Precise dielectric and conductive measurements would be helpful for further understanding. Using low-birefringent materials, the microscopic appearance of colloidal particles with the use of λ-plate leads to a drastic change in color with the onset of undulating dynamics. Here we consider that the periodic director distortion in the thickness direction due to the EHC is negligible. In other words, it is reasonable to assume that the director field is parallel to the glass substrates. [36] To understand the results qualitatively, we crudely separate the sample into three parts as shown in Figure 6. The regions near the top and bottom substrates (i), (iii) can be regarded as uniform NLC slabs in which the director is parallel to the rubbing direction. On the other hand, the director on both sides of the particle make an angle to the rubbing (x-) direction. Here we neglect the effect of the director distortion in z-direction. In the experimental condition, the linearly polarized light from the source enters the NLC slab (iii) that does not change the direction of polarization since the rubbing direction is parallel to the polarizer, while the distorted region (ii) causes a phase retardation of one ray to the other and, moreover, the NLC slab (i) also works as an optical retardation layer. Considering the effect of the distortion at the slab (ii) for the optical retardation is constant, it is obvious that the net retardation caused by the sample depends on z-position of the particle. Under cross-polarized condition, however, the orientation of the director field results in the same appearance. The direction of the fast and slow axes can be visualized with λ-plate. For instance, when the particle locates near the top substrate, the effect is mainly comes from the distorted region (ii). By λ-plate, one side add and the other side subtract the retardation, leading to bluish and yellowish colors as shown $t = 38/60$ s in Figure 2(D).[37] As the particle moves downward by the EHC flow, the NLC layer (C) further adds colors on both sides of the colloids. The microscopic appearance follows the Michel-Levy color chart. Arrows in Figure 2(D) are examples that show the corresponding colors in the same order appearing opposite side of particles. Detailed evaluation could be possible by using Jones matrix approach. Actually the idea can be applied to the colloidal chain. As mentioned, the undulating shape of the long chain in Figure 4 is obtained as a result of a gradual increase of the voltage. This means that the amplitude of the undulation is not so large as the single particle moving in Williams domains as shown in Figure 2(D). By taking this into account, we can see that the colors around the chain in Figure 4 correspond to $t = 9/60$ s and $t = 22/60$ s in Figure 2(D). Moreover, it is possible to explain the observation of Figure 5 where the chains attain the larger amplitude in z-direction. Because the larger volume is distorted by the particles connected nearly vertically, the large retardation shifts to the higher order of the interference color chart.

To conclude, using a NLC with low birefringence, we found that the microscopic appearance of the colloidal particles in the EHC is quite distinctive with the use of λ-plate. The observed color around the particles can be attributed to the change in retardation determined by its height, which is actually in agreement with the interference color chart. Considering the increasing attention for liquid crystal microfluidics, [18, 19] our approach would be useful for such a purpose because of the simplicity. In the present system, the horizontal roll width is narrow for the cell thickness. The expansion of the size by controlling physical properties would be more interesting and helpful for

further understanding.

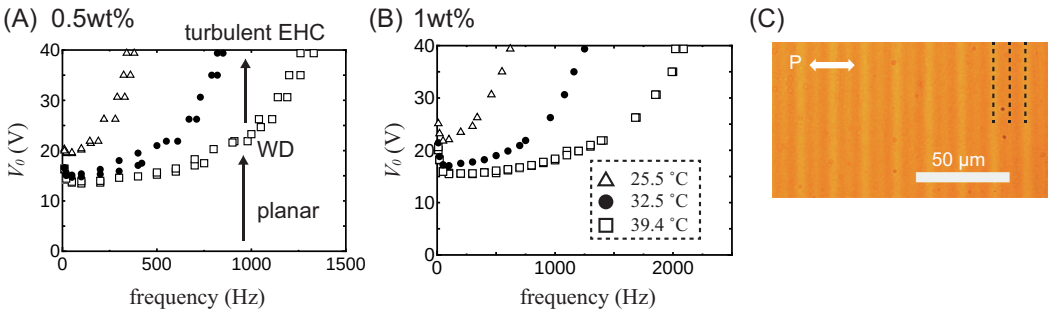

Figure 1. (A), (B) The threshold voltage V_0^{th} as a function of applied frequencies for two ionic concentrations. (C) A micrograph of Williams domains of (B) under plane-polarized illumination at 20 Hz and 25.5°C. The dashed lines are a guide to the eyes for the boundary of rolls.

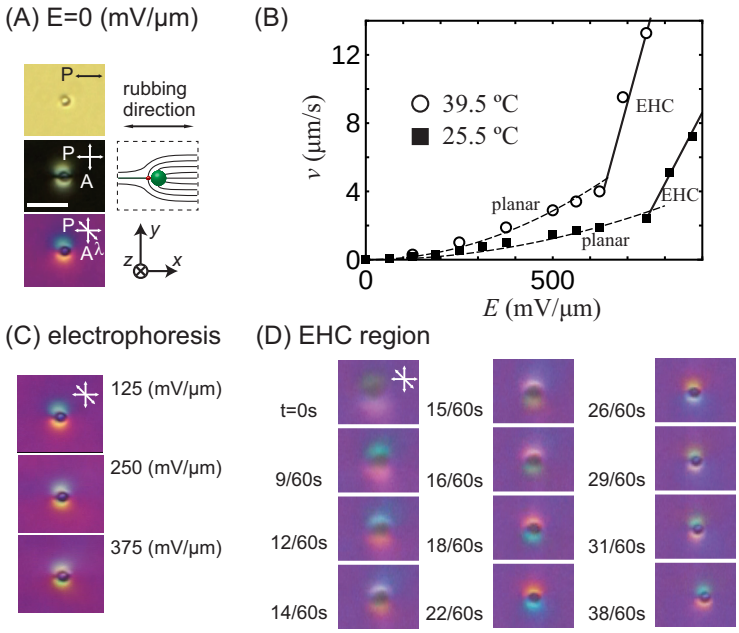

Figure 2. (A) Micrographs of a single dipolar particle under different illuminations. Scale bar; 10μm. P, A, λ denote the polarizer, analyzer, and λ-plate, respectively. The schematic illustration shows the director distortion around the particle. (B) The x-directional speed of a particle depending on the electric field strength. The frequency used here is 20 Hz. The dashed quadratic curves in lower electric fields correspond to the electrophoretic motion. On the other hand, the solid straight lines in high electric fields are a guide to eyes to show the EHC region. (C) Microscopic appearance of a single particle moving by electrophoresis. (D) Microscopic appearance of a single particle near a boundary of the EHC rolls. The amplitude of the electric field is 750 mV/μm. Since the particle moves towards the upper substrate, i.e., in the positive z-direction, the x-directional shift is small. The direction of the point defect is the same as (A). For (C), (D), the temperature of the sample is 39.5 °C.

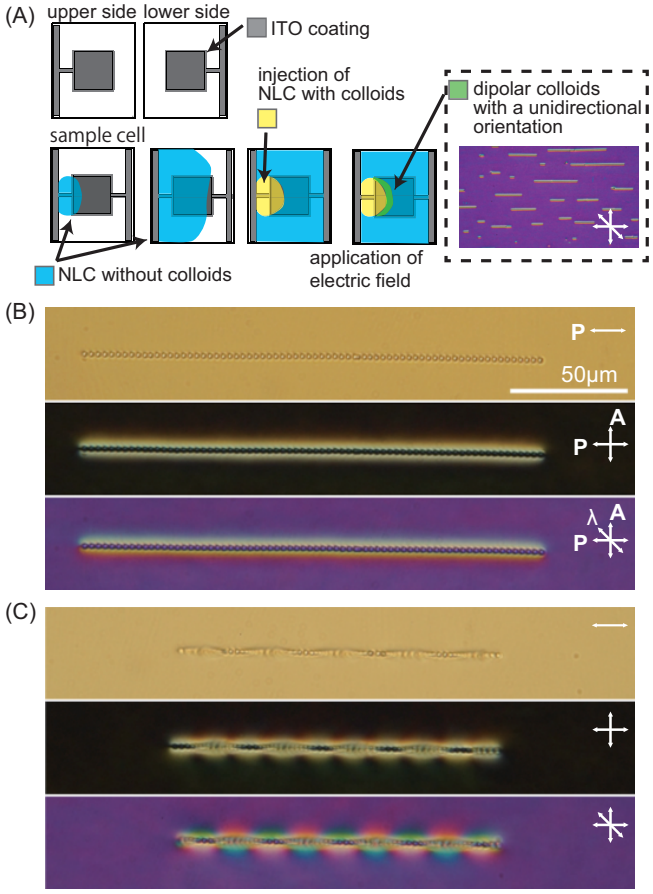

Figure 3. (A) Schematic illustration of sample preparation. (B) Micrographs of a chain. (C) The undulating chain by the local EHC in a lower voltage than V_0^{th}. The voltage here is $V_0 \sim 11$ V, $f = 20$ Hz. Scale bar; 50 μm.

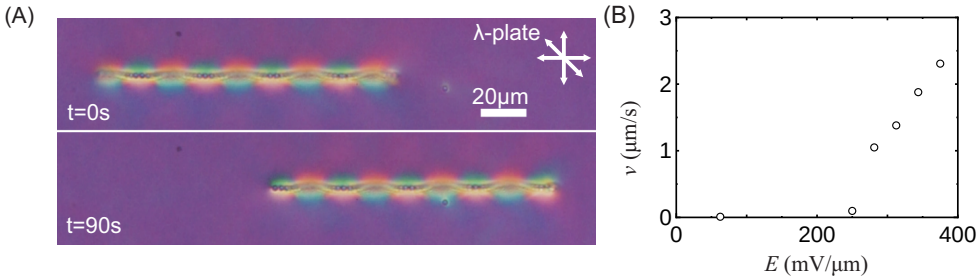

Figure 4. (A) Micrographs of an undulating structure consisting of $\sim$ 70 particles at 39.5 °C. The applied voltage here is $V_0 = 10.5$ V and $f = 20$ Hz. Images are taken under cross-polarized condition with λ-plate. (B) The speed dependence as a function of applied electric field. The further increase of the field leads to the breakage of chain.

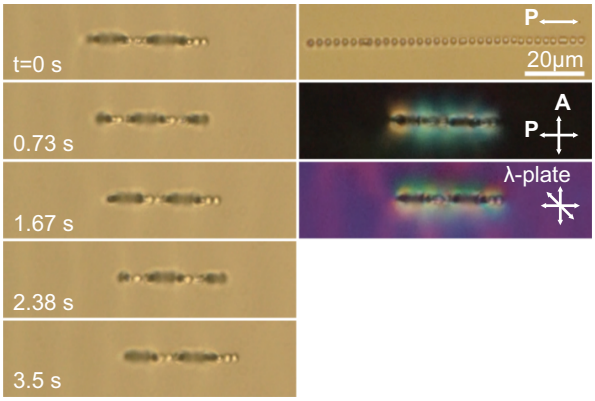

Figure 5. Snapshots of a chain moving in the EHC domains and typical micrographs taken under different conditions. The applied voltage is $V_0 = 16.6$ V, $f = 20$ Hz and the temperature is 39.5 °C.

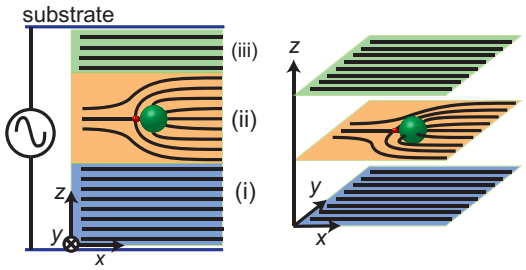

Figure 6. Schematic illustration of the director field in the cell. (i) and (iii) are regions where the director is parallel to the rubbing direction. The director is distorted around the particle in the region (ii).

Acknowledgement

This work was partly supported by a Grant-in-Aid for Scientific Research on Innovative Areas 'Fluctuation and Structure' (No. 25103006) from the Ministry of Education, Culture, Sports, Science, and Technology of Japan.

Supplemental material

Movie 1 (0.1× speed) shows an elastic dipole moving in EHC under cross-polarized condition with the insertion of a λ-plate. Movie 2 (1x speed) shows a chain in EHC under plane polarized condition.

References

[1] de Gennes PG, Prost J. The physics of liquid crystals. Oxford University Press; 1995.
[2] Pouline P, Stark H, Lubensky TC, Weitz DA. Novel colloidal interactions in anisotropic fluids. Science. 1997;275:1770–1773.
[3] Poulin P, Weitz DA. Inverted and multiple nematic emulsions. Phys Rev E. 1998;57:626–637.
[4] Muševič I. Integrated and topological liquid crystal photonics. Liq Cryst. 2014;41:418–429.
[5] Loudet JC, Barois P, Poulin P. Colloidal ordering from phase separation in a liquid-crystalline continuous phase. Nature. 2000;407:611–613.
[6] Muševič I, Škarabot M, Tkalec U, Ravnik M, Žumer S. Two-dimensional nematic colloidal crystals self-assembled by topological defects. Science. 2006;313:954–958.
[7] Nych A, Ognysta U, Škarabot M, Ravnik M, Žumer S, Muševič I. Assembly and control of 3d nematic dipolar colloidal crystals. Nat Commun. 2013;4:1489.
[8] Lavrentovich OD, Lazo I, Pishnyak OP. Nonlinear electrophoresis of dielectric and metal spheres in a nematic liquid crystal. Nature. 2010;467:947–950.
[9] Lavrentovich OD. Transport of particles in liquid crystals. Soft Matter. 2014;10:1264–1283.
[10] Lazo I, Lavrentovich OD. Liquid-crystal-enabled electrophoresis of spheres in a nematic medium with negative dielectric anisotropy. Phil Trans R Soc A. 2013;371:20120255.
[11] Bazant MZ, Squires TM. Induced-charge electrokinetic phenomena: theory and microfluidic applications. Phys Rev Lett. 2004;92:066101–1–066101–4.
[12] Gangwal S, Cayre OJ, Bazant MZ, Velev OD. Induced-charge electrophoresis of metallodielectric particles. Phys Rev Lett. 2008;100:058302–1–4.
[13] Lazo I, Peng C, Xiang J, Shiyanovskii SV, Lavrentovich OD. Liquid crystal-enabled electro-osmosis through spatial charge separation in distorted regions as a novel mechanism of electrokinetics. Nat Commun. 2014;5:5033.
[14] Dierking I, Biddulph G, Matthews K. Electromigration of microspheres in nematic liquid crystals. Phys Rev E. 2006;73:011702–1–6.
[15] Jákli A, Senyuk B, Liao G, Lavrentovich OD. Colloidal micromotor in smectic a liquid crystal driven by dc electric field. Soft matter. 2008;4:2471–2474.
[16] Takahashi K, Kimura Y. Dynamics of colloidal particles in electrohydrodynamic convection of nematic liquid crystal. Phys Rev E. 2014;90:012502–1–5.
[17] Hernàndez-Navarro S, Tierno P, Farrera JA, Ignés-Mullol J, Sagués F. Reconfigurable swarms of nematic colloids controlled by photoactivated surface patterns. Angew Chem Int Ed. 2014;53:10696–10700.
[18] Sengupta A, Bahr C, Herminghaus S. Topological microfluidics for flexible micro-cargo concepts. Soft Matter. 2013;9:7251–7260.
[19] Sengupta A. Topological constraints in a microfluidic platform. Liq Cryst. 2014;41:290–301.
[20] Williams R. Domains in liquid crystals. J Chem Phys. 1963;39:384–388.
[21] Buka A, Kramer L. Pattern formation in liquid crystals. Springer; 1996.
[22] Sasaki Y, Takikawa Y, Jampani V, Hoshikawa H, Seto T, Bahr C, Herminghaus S, Hidaka Y, Orihara H. Colloidal caterpillars for cargo transportation. Soft Matter. 2014;10:8813–8820.
[23] Sasaki Y, Hoshikawa H, Seto T, Kobayashi F, Jampani V, Herminghaus S, Bahr C, Orihara H. Direct

visualization of spatiotemporal structure of self-assembled colloidal particles in electrohydrodynamic flow of a nematic liquid crystal. Langmuir. 2015;31:3815–3819.
[24] Kaiser A, Babel S, ten Hagen B, von Ferber C, Löwen H. How does a flexible chain of active particles swell? J Chem Phys. 2015;142:124905–1–124905–8.
[25] Ramírez LM, Michaelis CA, Rosado JE, Pabón EK, Colby RH, Velegol D. Polloidal chains from self-assembly of flattened particles. Langmuir. 2013;29:10340–10345.
[26] Sai DV, Kumar TA, Haase W, Roy A, Dhara S. Effect of smectic short-range order on the discontinuous anchoring transition in nematic liquid crystals. J Chem Phys. 2014;141:044706–1–044706–6.
[27] Sai DV, Zuhail K, Sarkar R, Dhara S. Structure-property correlation of bicyclohexane nematic liquid crystals. Liq Cryst. 2015;42:328–333.
[28] Rasna M, Zuhail K, Manda R, Paik P, Haase W, Dhara S. Discontinuous anchoring transition and photothermal switching in composites of liquid crystals and conducting polymer nanofibers. Phys Rev E. 2015;89:052503–1–052503–5.
[29] Pishnyak OP, Tang S, Kelly JR, Shiyanovskii SV, Lavrentovich OD. Levitation, lift, and bidirectional motion of colloidal particles in an electrically driven nematic liquid crystal. Phys Rev Lett. 2007; 99:127802–1–4.
[30] Hernàndez-Navarro S, Tierno P, Ignés-Mullol J, Sagués F. Ac electrophoresis of microdroplets in anisotropic liquids: Transport, assembling and reaction. Soft Matter. 2013;9:7999–8004.
[31] Dhara S, Madhusudana N. Physical characterisation of 4′-butyl-4-heptyl-bicyclohexyl-4-carbonitrile. Phase Transit. 2008;81:561–569.
[32] Kochowska E, Németh S, Pelzl G, Buka Á. Electroconvection with and without the carr-helfrich effect in a series of nematic liquid crystals. Phys Rev E. 2004;70:011711–1–011711–9.
[33] Tóth-Katona T, Cauquil-Vergnes A, Éber N, Buka Á. Nonstandard electroconvection with hopf bifurcation in a nematic liquid crystal with negative electric anisotropies. Phys Rev E. 2007;75:066210–1–066210–12.
[34] Krekhov A, Pesch W, Éber N, Tóth-Katona T, Buka Á. Nonstandard electroconvection and flexoelectricity in nematic liquid crystals. Phys Rev E. 2008;77:021705–1–021705–10.
[35] Carr EF. Conductivity anisotropy in p-n-nonyloxybenzoic acid. Phys Rev A. 1975;12:327–329.
[36] Rasenat S, Hartung G, Winkler BL, Rehberg I. The shadowgraph method in convection experiments. Exp Fluids. 1989;7(6):412–420.
[37] Murphy DB, Davidson MW. Fundamentals of light microscopy and electronic imaging, 2nd edition. Wiley-Blackwell; 2012.